ACS APPLIED MATERIALS & INTERFACES

Research Article

www.acsami.org

Reinforcement of Stereolithographic Resins for Rapid Prototyping with Cellulose Nanocrystals

Sandeep Kumar,[†] Manfred Hofmann,[‡] Bettina Steinmann,[‡] E. Johan Foster,*[,†] and Christoph Weder*[,†]

[†]Adolphe Merkle Institute, University of Fribourg, Route de l'Ancienne Papeterie, 1723 Marly, Switzerland

[‡]3D Systems S.A., Route de l'Ancienne Papeterie, 1723 Marly, Switzerland

Supporting Information

ABSTRACT: We report on the mechanical properties of optically curable stereolithographic resins (SLRs) which were reinforced through the addition of small amounts of cellulose nanocrystals (CNCs). The resin/filler mixtures are readily accessible via simple mixing processes. A detailed rheological investigation of such mixtures and the successful processing of these materials on a commercial SLR machine show that at low filler concentrations (below 5%) the processability of the materials is barely impacted. The storage modulus, E', increased steadily with increasing CNC content in the regimes below and above the glass transition. A remarkable modulus enhancement was observed in the rubbery regime, where E' increased by 166, 233, and 587% for CNC/SLR nanocomposites with 0.5, 1.0, and 5.0% w/w CNC, respectively. The modulus increase was less pronounced in the glassy state, where E' increased by 21, 32 and 57%, for the same compositions. The increase in tensile strength was of similar magnitude. In comparison to previously reported CNC and carbon-nanofiller based nanocomposites, the presently investigated nanocomposites display a comparably large increase of stiffness and strength, which appear to originate from the high level of dispersion and the intimate contact of the CNCs with the SLR matrix. Through the fabrication of 3-dimensional parts, it was shown that the CNC-filled resins can be processed with standard equipment in a stereolithographic process that is widely used for rapid prototyping and rapid manufacturing.

KEYWORDS: *cellulose nanocrystals (CNC), mechanical reinforcement, polymer nanocomposites, stereolithography resins (SLR), stereolithography, rapid prototyping*

INTRODUCTION

In the past 25 years, significant efforts have been devoted to the development of polymer nanocomposites, in which the incorporation of a rigid, high-aspect-ratio nanofiller such as clay or carbon nanotubes (CNT), improves the mechanical, thermal, or other properties of the polymer. Since their first demonstrated use as reinforcing filler in the mid-1990s, cellulose nanocrystals (CNCs, also referred to as cellulose nanowhiskers, nanocrystalline cellulose, cellulose microcrystals, and rodlike cellulose crystals) have been extensively investigated due to their interesting mechanical properties and potential technological applications as reinforcing filler in a broad range of polymers.[1−7] CNCs are produced by selective acid hydrolysis of natural cellulosic materials (e.g., wood, cotton, sisal, tunicates), resulting in needlelike crystallites with diameters of 4−20 nm, and lengths of 100 nm to a few μm, depending on the source plant.[8] CNCs have a high surface area and high on-axis stiffness (Young's modulus of 100 to 143 GPa),[9,10] which make them ideal for polymer reinforcement. In comparison to other nanofillers, such as carbon nanotubes,[11] carbon nanofibers,[12,13] and graphene,[14] CNCs several advantages, including biosustainability, biorenewability, low production cost, and possibly lower cytotoxic and (pro-)inflammatory effects when inhaled.[15] Last but not least, CNCs offer simple functionalization and dispersibility, because of the surface chemistry based on carbohydrates, which can readily be modified.

Received: July 13, 2012
Accepted: September 19, 2012
Published: September 19, 2012

 © 2012 American Chemical Society

We here report on the reinforcement of a stereolithography resin for 3D printing, a technology that was first introduced by Charles W. Hull,[16] and which is now widely used for rapid prototyping and manufacturing. The general process involves building up objects of virtually any desirable shape, by optically curing a liquid resin in a layer-by-layer fashion (Figure 1).[17−19]

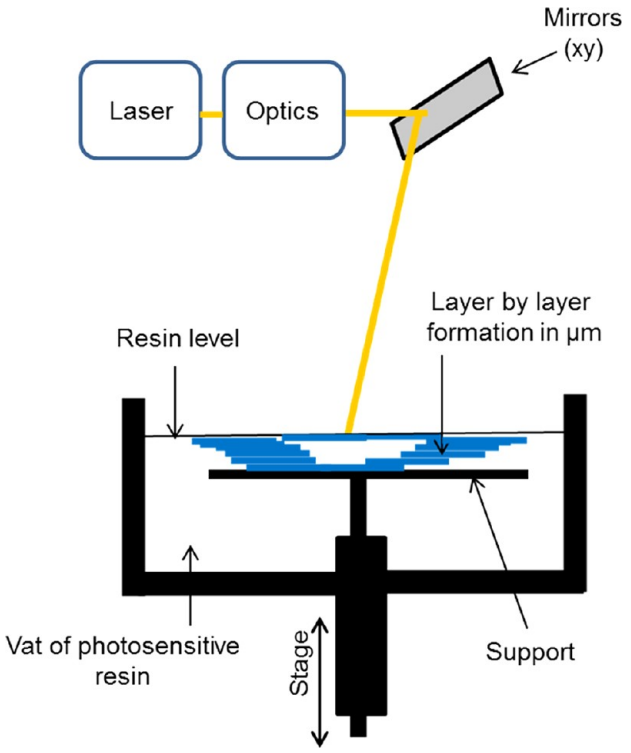

Figure 1. Schematic representation of the stereolithography process. Optically curing a liquid resin in a layer-by-layer fashion allows for the fabrication of three-dimensional objects of any desirable shape.

This is achieved by gradually lowering a platform in a reservoir of the optically curable resin, and polymerizing the surface resin layer in a spatially resolved manner with a computer-controlled laser. After each writing step, the platform is lowered by a small increment so that the just-created polymer layer is brought below the resin level and the next layer is written.[17,20] Typical stereolithography resin (SLR) formulations are based on either a cationically curable monomer or prepolymer or a combination of monomers/prepolymers that can be cured by cationic (e.g., epoxy, oxetane) and free radical (e.g., oligoacrylate) mechanisms.[21] If orthogonal chemistries are used, the photopolymerization results in an interpenetrating network of two different polymers.[22] Traditional SLR materials are highly cross-linked and thus generally rather brittle. They also feature low glass transition temperatures, which causes them to soften at moderate temperatures. Their unbalanced stiffness/toughness/heat stability profile limits their application especially in rapid manufacturing applications.[23] The improvement of the mechanical properties of SLRs for rapid prototyping and rapid manufacturing, as demonstrated in the present paper, is therefore a topic of interest. "Conventional" approaches for modifying the properties of SLRs include resin formulation, chemical modifications of the components, and the addition of (inorganic) fillers such as glass fibers, silica, and others. On account of its simplicity, the latter approach is particularly attractive, but it has been challenging to maintain a high level of transparency and high resolution of the writing process as the filler particles tend to absorb and/or scatter light. An obvious evolution that may address these issues is the use of nanoscale fillers. Gurr et al. reported an optically transparent SLR filled with up to 30% w/w silica nanoparticles and observed an increase of the Young's modulus of 25% at a nanofiller content of 17% w/w without significantly impacting the optical properties; a higher nanofiller increased the stiffness by another 7%, but the transparency was significantly reduced.[23] Liu and Mo utilized surface-modified silica nanoparticles with epoxide moieties that participate in the curing reaction and integrate with the polymer network.[21] The flexural modulus and tensile strength of the material filled with 1% w/w silica were reported to increase by 189 and 22.4%, respectively; for the resin filled with 2% w/w silica, the increases were 120 and 43.6%, respectively. Sandoval et al. investigated epoxy-based SLRs into which small amounts of multiwalled carbon nanotubes (MWCNTs) were incorporated. They observed an increase in tensile strength of 5.7 and 7.5% over the neat resin when 0.025 and 0.1% w/v CNTs were incorporated.[17]

We[9] and other groups[24−26] previously reported on reinforcing epoxy systems with different types of nanocellulose and observed a significant stiffness increase at filler contents in the range of 5−20% w/w. Interestingly, CNCs have, to our best knowledge, not been explored as a filler for SLRs. We note that to maintain good processability, the viscosity of SLR formulations must kept low, and therefore the content of high-aspect-ratio filler must be kept as small as possible. We therefore explored in a systematic study, how the introduction of small amounts of CNC, i.e., ≤ 5% w/w, would change the mechanical properties of optically curable SLR/CNC nanocomposites.

EXPERIMENTAL SECTION

SLR Composition. The SLR composition used here was a mixture of 3,4-epoxycyclohexylmethyl-3,4-epoxycyclohexanecarboxylate (Doublemer 421P; weight-average molecular weight, M_w = 352), a propoxylated polyether triol (Voranol CP 450; M_w = 204), ethoxylated pentaerythritol tetraacrylate (SR 494; M_w= 450), and trimethylolpropane oxetane (TMPO; M_w = 204). The cured resin has a density of 1.2 g/cm^3.

Isolation of Cellulose Nanocrystals (CNCs). Cellulose nanocrystals were isolated from cotton using a procedure that was described previously.[9] The CNC concentration in the resulting aqueous suspensions was determined gravimetrically to be 11−12 mg/mL. The CNC suspensions were freeze-dried to isolate dry CNCs.

Preparation of CNC/SLR Mixtures. The typical procedure for the preparation of CNC/SLR nanocomposites is described here for a composition containing 1.0% w/w of CNCs. The resin components (3,4-epoxycyclohexylmethyl-3,4-epoxycyclohexanecarboxylate (9.6 g), trimethylolpropane oxetane (3.0 g), glycerin propoxylated polyether triol (2.0 g), and ethoxylated pentaerythritol tetraacrylate (4.0 g)) were premixed in a beaker under ambient condition by stirring for 15 min with a magnetic stirrer at a speed of 500 rpm. The appropriate amount of lyophilized CNCs (0.22 g) was added, and the mixture was stirred at a speed of 700−800 rpm at 50 °C for another 30 min, and subsequently sonicated for 45 min at approximately 40 °C in an ultrasonic bath (VMR USC600TH/40kHz/120W). The curing agents Speedcure 976 (mixed triarylsulfonium hexafluoroantimonate salts dissolved in a mixture of propylene carbonate in a 50/50 (w/w) ratio) (0.8 g) and Speedcure 184 (1-hydroxycyclohexyl phenyl ketone) (0.6 g), were added and the mixture was stirred for 15 min at room temperature using a high shear disperser (EURO-STD/IKA-WERKE/60 Hz/75 W) at 1000 rpm. The mixture was again ultrasonicated for 15 min to remove any air bubbles; in cases where ultrasonication was not sufficient to remove the air bubbles, the mixture was placed for 5

min in a vacuum oven at pressure of 400 mbar to achieve a bubble-free suspension.

Rheological Studies. An Anton Paar Physica MCR300 rheometer with narrow gap concentric cylindrical geometry was used for the rheological measurement of CNC/SLR mixtures. The measurements were done in steady and dynamic states. Steady-state experiments were done over a shear rate range of 0.1 to 100 s^{-1} and frequency sweeps were performed in a frequency range of 0.01 to 100 rad/s.

Optical Curing of CNC/SLR Mixtures. Homogeneously cured films of a thickness of 0.2 mm were produced by casting the CNC/SLR mixture (9 g) into aluminum Petri dishes (diameter of 80 mm) and exposing the sample for a total of 20 min (releasing the partially cured sample from the mold after 10 min of exposure and turning it over) to a 400 W tungsten medium-pressure mercury lamp (Philips HPA 400 S in THORN EMI: ODW 500 housing) that was placed at a distance of 30 cm away from the sample. The light intensity measured at the sample surface of samples was ~180 mJ/cm^2 (264−360 nm). All optical curing experiments were carried out at ambient temperature in the presence of air. Samples used for tensile testing and the determination of flexural properties were made by casting the CNC/SLR mixtures into dog-bone and rectangular shape Teflon molds (ASTM standard D638). In this case, the samples had a thickness of 2.2 (tensile testing) and 4 mm (flexural testing) and were cured under the same conditions as the films described above. After curing, all samples were placed in desiccator to condition for standard humidity.

Fabrication of Three-Dimensional Parts by Stereolithography. The above preparation process was scaled up to 250 g to allow building of test parts (dog-bone shape) and three-dimensional parts in a sterolithographic process. A 3D Systems VIPER si^2 multimaterial machine was used to fabricate three-dimensional parts from the CNC/SLR resin containing 1.0% w/w CNCs. The machine was equipped with a solid-state laser with frequency conversion emitting at 355 nm with a power of 100 mW, a 1500 mL resin vat, and 9 × 11 cm^2 platforms. Before transferring the CNC/SLR mixture into the vat, the mixture was stirred and ultrasonicated as described above, but with slight modifications in ultrasonication time (increased to 2 h) to maximize the level of dispersion. After the object had been manufactured, the excess resin was drained off; to ensure complete removal of uncured resin from the surface, the part was rinsed with isopropanol for few minutes. The object was finally postcured for 1−2 h in an UV oven (model PCA-1, Lamp types TL-K40W/05 and TL-K40W/03, PHILIPS) in which samples were irradiated with light of a wavelength of 355 - 420 nm.

Transmission Electron Microscopy. The dimensions of the CNC and the quality of CNC dispersion in the CNC/SLR nanocomposites were studied by transmission electron microscopy (TEM) on a Philips CM 100 operating at an accelerating voltage of 80 kV. To analyze the size distribution of CNCs, the following experimental procedure was applied. Lyophilized CNCs were redispersed in water at a concentration of 0.1 mg/mL by ultrasonication in an ultrasonic bath (VMR USC600TH/40kHz/120W) for 5 to 10 min. Subsequently, a 10 μL drop of the aqueous CNC suspension was placed onto a copper grid, on which the CNCs were supported by 3 nm thick layer of carbon on top of a 50 nm layer-polymer membrane. The samples were then dried at 60 °C in a vacuum oven for 2 h. TEM images were then taken of these samples and the dimensions of 15−20 CNCs, from each of 5 TEM images, from 3 different batches of CNCs were determined; the averaged values are reported. To study the dispersion of CNCs in the nanocomposites, we cut CNC/resin films into slices of a thickness of 95 nm with an ultramicrotome (Leica), placed on copper grids, and TEM images were taken.

Dynamic Mechanical Analysis. The tensile storage modulus (E') and the tangent of the phase angle (tan δ) of the nanocomposite films were characterized as a function of temperature by dynamic mechanical analysis (DMA) using a TA Instrument DMA Q 800 model in thin film tension mode. The samples were subjected to an amplitude of 15 μm at a frequency of 1 Hz in the temperature range of 0−150 °C at a heating rate of 5 °C/min.

Tensile Testing. Dumbbell-shaped test samples (dimensions 70 × 4 × 2.2 mm^3) were used for tensile testing (ASTM: D638). Tensile tests were carried out using a Zwick tensile tester with a 10 kN load cell, at room temperature with an extension speed of 5 mm/min and an initial gauge length of 35 mm. The results reported are the averages of three samples for each nanocomposite.

Flexural Testing. Flexural tests were carried out on rectangular bars (80 × 10 × 4 mm^3, ASTM: D790) using a Zwick/Roell model Z010 flexural tester at room temperature.

RESULTS AND DISCUSSION

Preparation of CNC/SLR Mixtures. The SLR resin used in this study was a well-known hybrid system comprising a cationically curable monomer combination (3,4-epoxycyclohexylmethyl-3,4-epoxycyclohexanecarboxylate and a glycerin propoxylated polyether triol) and ethoxylated pentaerythritol tetraacrylate, which can be polymerized by a free-radical mechanism (Figure 2).[27] The hybrid chemistry leads to an

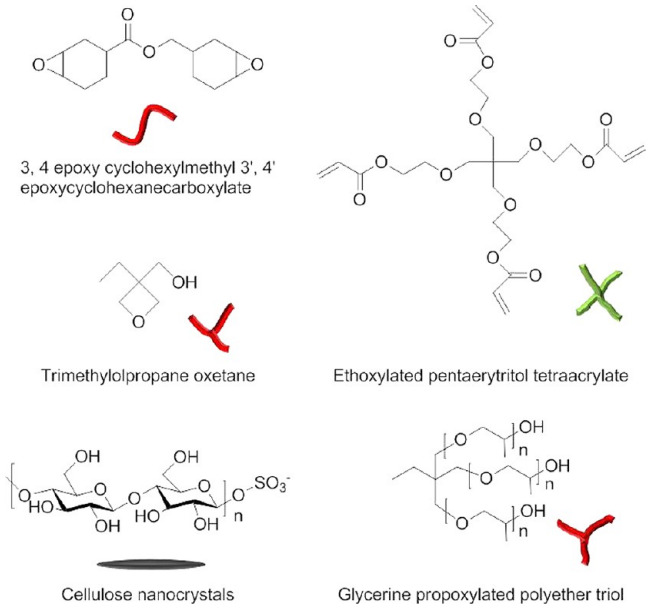

Figure 2. Chemical structures of the monomers used as components for the stereolithography resin (SLR) and of cellulose nanocrystals (CNCs) isolated via sulfuric acid hydrolysis of cotton cellulose pulp. Graphic representations of these species as they are used in Figure 3 are also included.

interpenetrating network consisting of an independent network formed by the free radical polymerization of the acrylic monomer and a network formed through the cationic polymerization of the epoxide monomer, trimethylolpropane oxetane and the polyether triol, respectively. It can be expected that the surface hydroxyl groups of the CNCs react with the epoxide in a manner similar to that of the polyether triol, which is one reason for the selection of this system (Figure 3). Further, the system was chosen because ultraviolet (UV) photocurable stereolithography resins offer quick setting and very high dimensional accuracy with good side wall surface finish. These resins systems are distinguished by very low viscosity, a very low curl factor (characterized by low shrinkage effects of an object), whereas many other resin systems prove to be very viscous and after photo curing do not satisfy the requirement of dimensional accuracy.[27]

The CNCs employed were isolated from cotton according to a previously published protocol.[7] The source was selected based

dx.doi.org/10.1021/am301321v | ACS Appl. Mater. Interfaces 2012, 4, 5399−5407

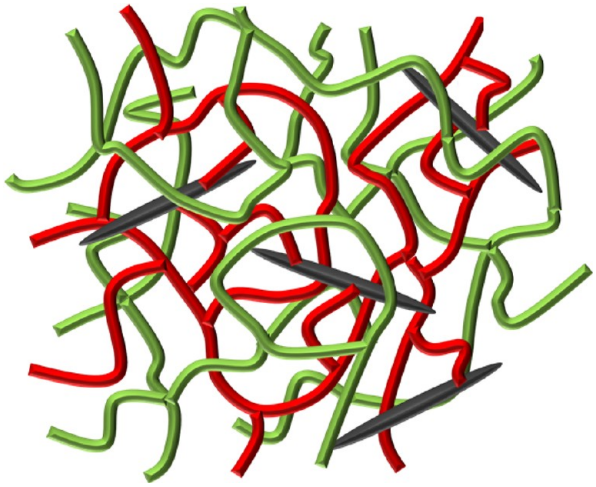

Figure 3. Interpenetrating network structure of the present SLR/CNC nanocomposites. Structural components are given in Figure 2. Two networks formed by free radical polymerization of the acrylic monomer (green) and a network formed through the cationic polymerization of the epoxide monomer (red) and CNCs (black) interpenetrate.

on its easy accessibility and the model character that many previous studies have given this CNC type. Transmission electron micrographs (Figure 4) provide information about the

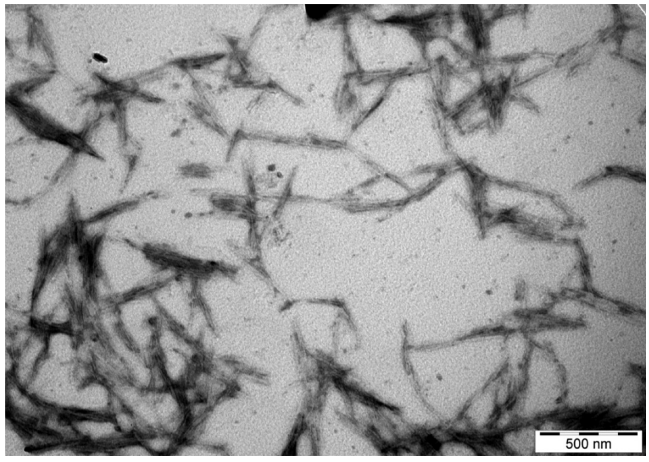

Figure 4. Transmission electron microscopy (TEM) image of cellulose nanocrystals (CNCs) isolated from cotton. For TEM imaging, lyophilized CNCs were redispersed in water at a concentration of 0.1 mg/mL and the suspension was deposited on TEM grids.

morphology of the CNCs and their dimensions. The evaluation of multiple TEM images (using image analysis software UTHSCSA Image Tool) results in an average length and diameter of 220 ± 61 and 15 ± 5 nm, respectively, and an average aspect ratio (length *l*/width *d*) of 12 (as determined from 5 TEM images of 3 different batches of CNCs). A bar graph that shows the length distribution is shown in the Supporting Information, Figure S1.

The typical procedure for the preparation of CNC/SLR dispersions involved mixing the monomers and an appropriate amount of lyophilized CNCs by mechanical stirring and subsequent ultrasonication, before the photoinitiators were added (see Experimental Section for details). The mixtures were further homogenized using a high shear disperser, and gas bubbles were removed by either brief ultrasonication or the application of vacuum. CNC/SLR mixtures with a CNC content of up to 5% w/w were studied in detail.

Rheological Characterization. To explore to what extent the introduction of the rigid, high-aspect-ratio CNCs impacts the processability of the SLRs on account of an increased viscosity, rheological studies were conducted. A plot of the viscosity versus the shear rate shows almost no change in viscosity with increasing shear rate for the neat resin and a dispersion containing 0.5% CNCs (Figure 5). Gratifyingly, the

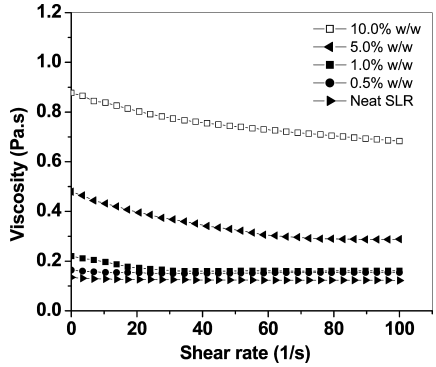

Figure 5. Chart showing the viscosity of uncured CNC/SLR mixtures as a function of shear rate and CNC content (all data acquired at 25 °C).

introduction of CNCs only caused a moderate viscosity increase, which increased with CNC content, e.g., from 0.13 (neat SLR) to 0.89 Pa·s (10% w/w CNCs) at a shear rate of 0.01 s^{-1}. Mixtures with a CNC content of 1.0% w/w or higher show distinct shear thinning behavior, which is likely due to an increasing alignment of CNCs as the shear rate increases.

The changes in storage modulus (G') and loss modulus (G'') of the CNC/SLR mixture as a function of frequency and CNC content are shown in Figure 6. As expected, both G' and G'' of the neat resin increase with increasing frequency in an essentially linear fashion. Both moduli increase upon introduction with CNCs. It can be seen that the frequency dependence of G' and G'' is dampened upon introducing CNCs, i.e., the slopes of the G' and G'' vs frequency traces eventually decrease compared to those of the neat resin. The difference is most pronounced for compositions with CNC content of 1.0% w/w or more in case of G' and 5.0% w/w or more in case of G'', suggesting a transition from a liquid-like to solid-like state. These findings are similar to observations previously reported for CNT/poly(ethylene terephthalate) and CNT/polypropylene nanocomposites[28,29] and are attributed to the formation of a stress-transferring filler network.[21] The values of different rheological parameters are tabulated in Table S1 in the Supporting Information. An increased degree of dispersion can be seen from the values of the flow index, which decreases with increasing CNC content.

A more precise description of the nanofiller concentration above which a rheological nanofiller network is formed and where the rheological properties increase in an exponential way can be determined using a power-law relationship[30]

$$G' \propto (m - m_c)^{\beta_c} m > m_c \quad (1)$$

where β_c is the critical exponent, which can be extracted from the slope of the log–log plot of G' vs $(m - m_c)$, m is the mass fraction of CNCs (% w/w) and m_c is the critical mass fraction

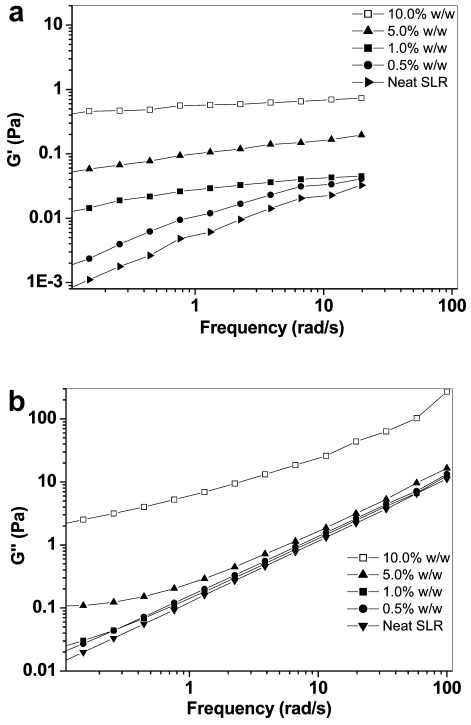

Figure 6. Charts showing (a) the storage modulus G' and (b) the loss modulus G'' of uncured CNC/SLR mixtures as a function of frequency and CNC content (all data acquired at 25 °C).

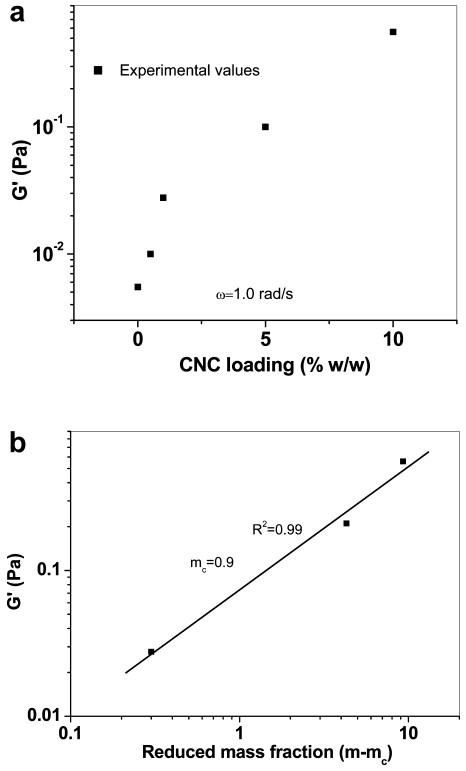

Figure 7. Charts showing the storage modulus (G') of uncured CNC/SLR mixtures as (a) a function of CNC content at a fixed frequency of 1.0 rad/s and (b) as a function of reduced mass fraction $m - m_c$. The solid line shown in (b) is a least-squares fit to the data, from which $m - m_c$ and therewith the critical mass fraction for rheological percolation threshold, m_c, were determined.

for rheological percolation threshold. A least-squares fit with m_c as a free parameter resulted an m_c of 0.9% w/w (Figure 7). This value is comparable to previously reported results of melt rheology of nanocomposites (m_c = 1.0−1.5% w/w) for CNCs derived from alfa fibers (l = 220 ± 20 nm and d = 8 ± 2 nm) in a poly(styrene-co-hexylacrylate) copolymer.[31] The rather low onset of rheological network formation can be directly linked to interactions between the resin and the CNCs and an excellent, uniform dispersion of the nanocrystals within the resin, which impedes the resin molecules mobility in a noticeable way. There are many reports available in literature which have shown that interfiller distance needed for rheology is longer, meaning that fewer fillers are required to approach the rheological network formation, than for solid state percolation network studied extensively in CNC work above 5.0% w/w CNCs.[9,29,30]

Optical Curing of CNC/SLR Mixtures. Homogeneously cured films of a thickness of 0.2 mm thickness were produced by casting the CNC/SLR mixtures into molds and exposing the samples for a total of 20 min to the light of a medium-pressure mercury lamp. The light intensity measured at the sample surface of samples was ∼180 mJ/cm^2.

Morphological Characterization. The morphology of the optically cured CNC/SLR nanocomposites was investigated by TEM imaging of ultrathin (95 nm) microtomed films. Figure 8 shows the corresponding TEM images of nanocomposites with a CNC content of 1.0 and 5.0% w/w. Gratifyingly, both images reveal a homogeneous dispersion of CNCs in the polymer matrix, confirming that the approach of directly mixing the lyophilized CNCs with the resin was indeed rather successful. It appears that at a content of 5.0% w/w CNCs, loosely aggregated CNCs start to appear (Figure 8), suggesting that the dispersion limit has been reached at this concentration.

Mechanical Properties. The mechanical properties of the cured CNC/CLR nanocomposites were characterized by dynamic mechanical analysis (DMA), tensile tests, and flexural tests. The results are shown in Figures 9 and 10 and Table 1.

The storage moduli E' of the neat SLR and the nanocomposites as a function of temperature were determined by DMA and are shown in Figure 9. The traces clearly revealed that the storage modulus of the CNC/SLR nanocomposites increased steadily with increasing CNC content at all temperatures. The data show a remarkable modulus enhancement in the rubbery regime, where (at 120 °C) E' increased from 0.033 GPa (neat SLR) by 166 (to 0.088 GPa), 233 (to 0.11 GPa), and 587% (to 0.23 GPa) for CNC/SLR nanocomposites with 0.5, 1.0, and 5.0% w/w CNC, respectively (Table 1). Because thermal degradation of the CNCs is an issue above 130 °C, where samples were found to yellow, values are reported at 120 °C and not T_g + 50 °C, as it is customary. However, we wish point out that although the absolute numbers decrease at higher temperatures, the relative improvement and trend remain similar. The modulus increase was less pronounced in the glassy state, where at 25 °C, E' increased by 21 (to 3.2 GPa), 32 (to 3.8 GPa) and 57% (to 4.3 GPa), for the same compositions. It is evident from Figure 9 that the introduction of CNCs also results in a higher usage temperature.

The room-temperature mechanical properties (i.e., in the glassy state) were further explored by tensile testing of UV-cured dumbbell-shaped specimen of the CNC/SLR nanocomposites (Figure 10). The data show an increase in Young's modulus from 3.1 GPa for the neat resin to 4.1 GPa for the nanocomposite with 5% w/w CNCs and confirm the findings of the DMA experiments. The tensile strength increased from

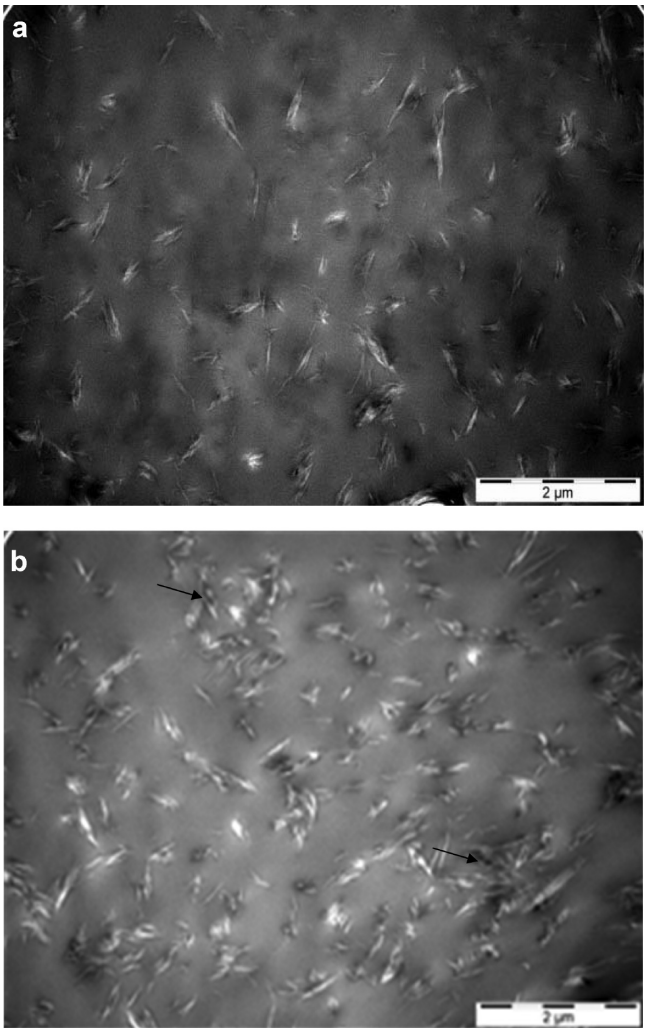

Figure 8. TEM images of cured CNC/SLR nanocomposites containing (a) 1.0 and (b) 5.0% w/w of CNCs. The black arrows indicate the formation of aggregates at a CNC content of 5.0% w/w.

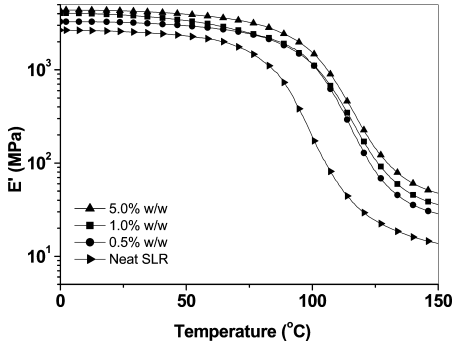

Figure 9. Chart showing the storage modulus (E') of cured CNC/SLR nanocomposites as a function of temperature and CNC content.

69 MPa for the neat resin to 77 and 82 MPa for CNC/SLR nanocomposite with CNC content of 1.0% and 2.0% w/w, respectively (Table 1). A further increase of the CNC content to 5.0% w/w had a detrimental effect on the tensile strength, perhaps due to the formation of CNC aggregates (cf. also Figure 8), which may act as stress concentrators that lead to increased brittleness, and reduce the elongation at break (vide infra).[32]

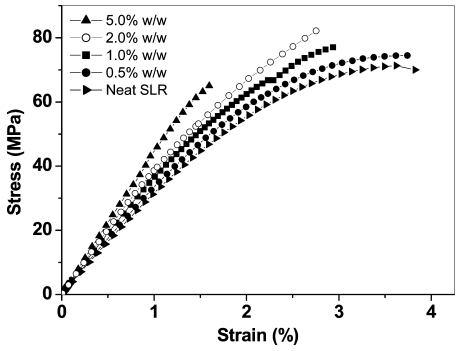

Figure 10. Chart showing the stress–strain curves of cured CNC/SLR nanocomposites as a function of CNC content (all data acquired at 25 °C).

Table 1. Mechanical Properties of Cured CNC/SLR Nanocomposites

	neat SLR	0.5% w/w CNC 0.39% v/v CNC	1.0% w/w CNC 0.77% v/v CNC	2.0% w/w CNC 1.55% v/v CNC	5.0% w/w CNC 3.89% v/v CNC
tensile strength (MPa)	69	74	77	82	65
Young's modulus (GPa)	3.1	3.4	3.6	3.9	4.1
elongation at break (%)	3.8	3.7	2.8	2.6	1.6
flexural modulus (GPa)	2.7	3.0	3.2	3.3	3.1
storage modulus at 25 °C(GPa)	2.6	3.2	3.8	n.a.	4.3
storage modulus at 120 °C(GPa)	0.033	0.088	0.11	n.a.	0.23
T_g (°C)	95	98	104	n.a	107

Flexural tests were performed to study the effect of CNCs on the bending properties of CNC/SLR nanocomposites (Table 1). The flexural modulus increased from 2.7 GPa for the neat resin to 3.3 GPa for a nanocomposite with a CNC content of 2.0% w/w. Again, a further increase of the CNC content to 5.0% w/w had a detrimental effect—the nanocomposite showed a slightly lower flexural modulus (3.1 GPa) than the materials with 2% CNCs.

We and many other researchers have previously used the Halpin–Tsai model to express the Young's modulus, $E_{composite}$, of a broad range of polymer/CNC nanocomposites as a function of filler content. The experimental Young's moduli of the present materials are well described by the model up to a CNC content of ca. 1.0% w/w, whereas at higher CNC concentrations the experimental data are lower than predicted (Figure 11a). The observed deviation mirrors previous results, which have shown that the Halpin–Tsai model overestimates the modulus at increasing filler contents.[33] A fit of the experimental data for compositions with a CNC content of <1% w/w against the model results a CNC modulus, E_{CNC}, of 100 GPa, which matches well with established values (60–120 GPa for cotton CNC).[34] Since an underlying assumption of the Halpin–Tsai model is that the filler particles are uniformly dispersed in the matrix, one may speculate that the difference between experimental and predicted moduli at higher CNC content originates from the aggregation of CNCs. To address

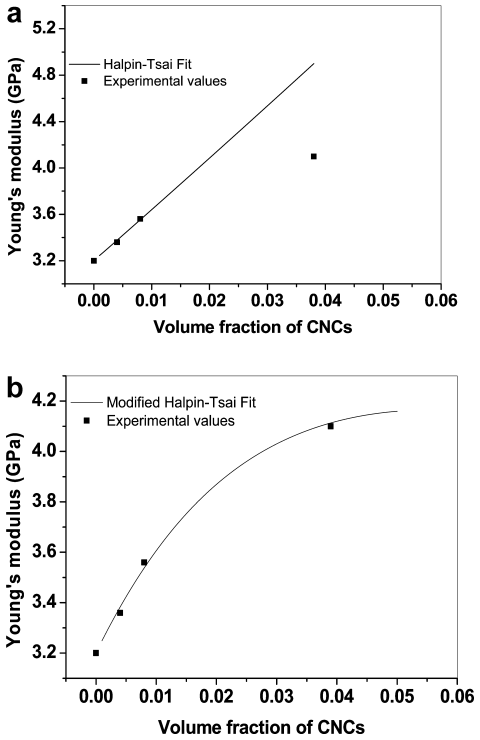

Figure 11. Experimental Young's moduli of cured CNC/SLR nanocomposites fitted by (a) Halpin–Tsai and (b) Modified Halpin–Tsai model with exponential shape factor for CNC/SLR nanocomposites.

this aspect, we explored the use of a Modified Halpin–Tsai model proposed by Yeh and Montazeri for multi walled carbon nanotubes MWCNT,[29] in which an exponential shape factor ψ was used to fit the nonlinear region observed for the filler contents of >1.0% w/w.[35,36] The exponential shape ψ factor has the form:

$$\psi = 2\left(\frac{l}{d}\right)e^{-av-b} \tag{2}$$

and is related to the aspect ratio l/d and v (volume fraction of CNC) in the Halpin–Tsai equation and a and b are constants that depend on the extent of aggregation of the nanofiller. The modified Halpin–Tsai equation can then be written as

$$\frac{1 + \left(2\left(\frac{l}{d}\right)e^{-av_{CNC}-b}\right)\eta v_{CNC}}{1 - \eta v_{CNC}}E_m \tag{3}$$

$$\eta = \frac{(E_{CNC}/E_m) - 1}{(E_{CNC}/E_m) + \psi} \tag{4}$$

where E_m is the modulus of matrix, E_{CNC} is the modulus of single cotton nanocrystal (100 GPa) and η is the efficiency factor. Using the modified Halpin–Tsai equation, the experimental values fit well with predicted values if the aggregation constants a and b are carefully adjusted (Figure 11b). Our results are in line with previous reports, showing that larger a fits the experimental values with predicted Young's modulus values at high CNC loadings, indicating more aggregation with increasing loading of CNC, while with increase in values of b, the Young's modulus of the nanocomposite samples decreases with higher loading of CNC.[36] A comparison of the values of the present CNC/SLR nanocomposites with those of previously studied systems (Table 3) reveals less aggregation for the CNCs, perhaps due to a lower aspect ratio relative to CNTs and better integration with the matrix. The small aggregation constants appear to correspond well with the qualitative information provided by the TEM images shown in Figure 8. This modified Halpin–Tsai equation seems to be very informative, as it can help to explain deviations from the idealized model, possibly due to varying degrees of aggregation in polymer systems, also allowing comparison of different composite compositions with respect to degree of presumed aggregation.

Table 2. Mechanical Data Comparison for SLR Reinforced with CNCs (this work) with Epoxy Resins Reinforced with 1% w/w CNFs, CNTs, or Graphene at Room Temperature

composite system	tensile strength (MPa) Composite (pure matrix) at 1.0% w/w	Young's modulus (GPa) composite (pure matrix) at 1.0% w/w	ref
epoxy/ graphene	59 (65)	2.8 (2.7)	14
epoxy/ carbon nanofibers	77(72)	2.8 (2.6)	13
epoxy/ carbon nanotubes	71 (64)	3.9 (3.4)	36
epoxy/ carbon nanotubes	72 (68)	3.6 (3.1)	11
CNCs/SLR	77 (69)	3.6 (3.1)	This work

Table 3. Values of Aggregation Constants from Modified Halpin–Tsai Model

composite system	(a)	(b)	ref
epoxy/CNT	150	1.5	36
epoxy/CNT	75	1.0	35
SLR/CNC	11.5	1.7	this work

Discussion of Mechanical Data in the Context of Previously Studied Nanocomposites. Several previous studies by our group and others revealed significant modulus increases for cotton-based CNC/polymer nanocomposites above T_g. For example, Mathew et al. reported an increase of E' of up to 49 and 143% in CNC/natural rubber composites comprising 2.5% and 10.0% w/w CNC, respectively.[37] Oksman et al. observed an increase of E' 100% and 332% for CNC/polyvinyl acetate (PVAc) and CNC/cellulose acetate butyrate nanocomposites with 5.0 and 6.0% w/w CNC, respectively.[32,38] Oksman et al. also studied the mechanical properties of CNCs/polylactic acid nanocomposites made by an extrusion process and reported an increase of E' of 70% and 240% at CNC contents of 1.0 and 3.0% w/w.[39] Tang et al. reported an increase of E' of 300 and 387% for CNCs/epoxy nanocomposites with 6 and 10.0% w/w CNCs, respectively.[9] In a recent article, Mendez et al. reported an increase of E' of 71% and 207% for CNCs/polyurethane nanocomposites comprising 4.0 and 7.0% v/v CNCs, respectively.[40] In light of these studies, the formidable reinforcement of 166, 233, and 587% displayed by the present CNC/SLR nanocomposites with 0.5, 1.0, and 5.0% CNCs, respectively is quite remarkable and consistent with the fact that (i) at these concentrations the CNCs are well-dispersed in the SLR and (ii) strong interactions between the CNCs and the SLR exist, perhaps via covalent bonds to the

epoxy-part of the resin. The effect that the introduction of CNC has on the tensile strength of the present SLRs is equally impressive, when compared to that of the above-referred materials (see Tables S2 and S3 in the Supporting Information). Interestingly, the reinforcement of the present SLRs with 1% w/w CNCs is comparable to the improvement that can be achieved in epoxy systems with carbon nanofibers, carbon nanotubes, or graphene (Table 2).[11,13,14,36] From this point of view, CNCs appear to be an exceedingly attractive alternative to other fillers, not only because of their lower costs and renewable nature, but also due to their reinforcing capabilities, which appear to originate from the high level of dispersion and the intimate contact with the polymer matrix.

Fabrication of Three-Dimensional Objects by Stereolithography. To probe the usefulness of the presently studied materials, we fabricated several 3D objects, both ASTM standard pieces for mechanical testing and purely demonstrative objects, using an SL approach. Thus, a 1.0% w/w CNC/SLR mixture was processed on a commercially available, 3D Systems Viper si^2 multimaterial machine (Figure 12). Gratifyingly, the process afforded CNC/SLR nanocomposite parts with intricate features (Figure 12). To study the mechanical properties of the materials made by the SL process, dog-bone shaped samples were also produced. The mechanical data show that the CNC/SLR nanocomposites fabricated by the SL process have indeed a similar strength (68 MPa) and higher stiffness (3.6 GPa) than reference samples made from the neat SLR (66 MPa and 3.2 GPa). Although the stiffness matched that of the samples cured in bulk, no improvement in strength was seen (77 MPa for the bulk material). The reason for this difference is still unclear; it may be related to the difference in irradiance (181 mJ/cm^2 and ~45 mJ/cm^2 for samples cured in bulk and with the SL process, respectively), but also reflect defects in the samples. We note that the SL process has little been optimized and speculate that further optimization should push the properties of the materials made by the stereolithographic process to the level seen in the optically cured bulk materials reported above.

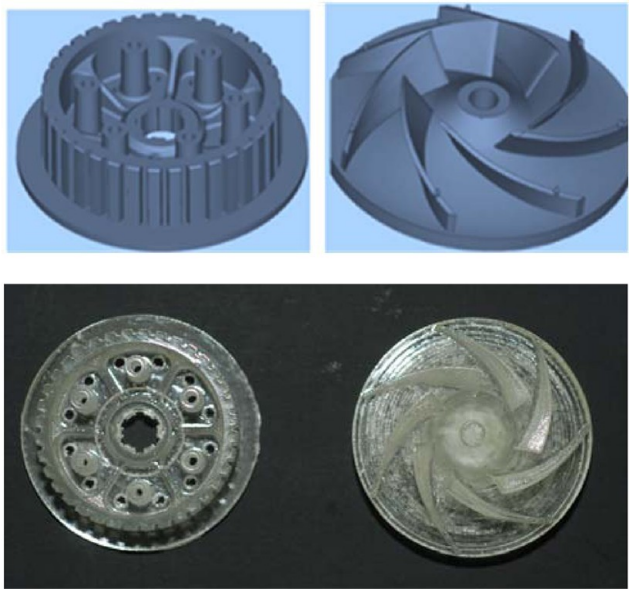

Figure 12. CAD designs (top) and parts (bottom) of a belt pulley (left) and water pump impeller (right). The objects were made for demonstration purposes with the stereolithography process show in Figure 1 from CNC/SLR mixture with 1.0% w/w CNCs.

CONCLUSIONS

In summary, we have shown that the mechanical properties of SLRs can be significantly increased through the addition of minute amounts of CNCs. The resin/filler mixtures are readily accessible by simple mixing processes. A detailed rheological investigation of such mixtures and the successful processing of these materials on a commercial SLR machine show that at such low filler concentrations the processability of the materials is hardly impacted. In comparison to previously reported CNC and carbon-nanofiller-based nanocomposites, the presently investigated nanocomposites display a comparably large increase of stiffness and strength, which appear to originate from the high level of dispersion and the intimate contact of the CNCs with the SLR matrix. Through the fabrication of three-dimensional parts, it was shown that the CNC-filled resins can be processed with standard equipment in a stereolithographic process.

ASSOCIATED CONTENT

Supporting Information

Plot showing the size distribution of CNCs used, rheological data for CNC/SLR mixtures as well as comparisons of the present system mechanical properties with other current polymer/filler systems. This material is available free of charge via the Internet at http://pubs.acs.org.

AUTHOR INFORMATION

Corresponding Author

*E-mail: johan.foster@unifr.ch; christoph.weder@unifr.ch.

Notes

The authors declare no competing financial interest.

ACKNOWLEDGMENTS

We gratefully acknowledge support from the Swiss Commission for Technology and Innovation (CTI) under Grant 11234.1 PFIW-IW and the Adolphe Merkle Foundation. We also acknowledge the use of instrumentation acquired with R'Equip funding from the Swiss National Science Foundation under Grant 206021_128728.

REFERENCES

(1) Favier, V.; Chanzy, H.; Cavaillé, J. Y. *Macromolecules* **1995**, *28*, 6365.
(2) Samir, M. A. S. A.; Alloin, F.; Sanchez, J. Y.; Dufresne, A. *Polymer* **2004**, *45*, 4149.
(3) Chazeau, L.; Cavaillé, J. Y.; Canova, G.; Dendievel, R.; Boutherin, B. *J. Appl. Polym. Sci.* **1999**, *71*, 1797.
(4) Ljungberg, N.; Bonini, C.; Bortolussi, F.; Boisson, C.; Heux, L.; Cavaillé, J. Y. *Biomacromolecules* **2005**, *6*, 2732.
(5) Capadona, J. R.; Van Den Berg, O.; Capadona, L. A.; Schroeter, M.; Rowan, S. J.; Tyler, D. J.; Weder, C. *Nat. Nanotechnol.* **2007**, *2*, 765.
(6) Capadona, J. R.; Shanmuganathan, K.; Tyler, D. J.; Rowan, S. J.; Weder, C. *Science* **2008**, *319*, 1370.
(7) Capadona, J. R.; Shanmuganathan, K.; Trittschuh, S.; Seidel, S.; Rowan, S. J.; Weder, C. *Biomacromolecules* **2009**, *10*, 712.
(8) Moon, R. J.; Martini, A.; Nairn, J.; Simonsen, J.; Youngblood, J. *Chem. Soc. Rev.* **2011**, *40*, 3941.
(9) Tang, L. M.; Weder, C. *ACS Appl. Mater. Interfaces* **2010**, *2*, 1073.
(10) Samir, M. A. S. A.; Alloin, F.; Dufresne, A. *Biomacromolecules* **2005**, *6*, 612.

(11) Ayatollahi, M. R.; Shadlou, S.; Shokrieh, M. M.; Chitsazzadeh, M. *Polym. Test* **2011**, *30*, 548.
(12) Choi, Y. K.; Sugimoto, K.; Song, S. M.; Gotoh, Y.; Ohkoshi, Y.; Endo, M. *Carbon* **2005**, *43*, 2199.
(13) Zhu, J. H.; Wei, S. Y.; Ryu, J.; Budhathoki, M.; Liang, G.; Guo, Z. H. *J. Mater. Chem.* **2010**, *20*, 4937.
(14) Zaman, I.; Phan, T. T.; Kuan, H. C.; Meng, Q. S.; La, L. T. B.; Luong, L.; Youssf, O.; Ma, J. *Polymer* **2011**, *52*, 1603.
(15) Clift, M. J. D.; Foster, E. J.; Vanhecke, D.; Studer, D.; Wick, P.; Gehr, P.; Rothen-Rutishauser, B.; Weder, C. *Biomacromolecules* **2011**, *12*, 3666−3673.
(16) Hull, C. W. U.S. Patent, 1986.
(17) Sandoval, J. H.; Wicker, R. B. *Rapid Prototyping J.* **2006**, *12*, 292.
(18) Sandoval, J. H.; Soto, K. F.; Murr, L. E.; Wicker, R. B. *J. Mater. Sci.* **2007**, *42*, 156.
(19) Choi, J. W.; Kim, H. C.; Wicker, R. *J. Mater. Process. Technol.* **2011**, *211*, 318.
(20) Badev, A.; Abouliatim, Y.; Chartier, T.; Lecamp, L.; Lebaudy, P.; Chaput, C.; Delage, C. *J. Photochem. Photobiol., A* **2011**, *222*, 117.
(21) Liu, H. T.; Mo, J. H. *J. Reinf. Plast. Compos.* **2010**, *29*, 909.
(22) Sangermano, M.; Carbonaro, W.; Malucelli, G.; Priola, A. *Macromol. Mater. Eng.* **2008**, *293*, 515.
(23) Gurr, M.; Hofmann, D.; Ehm, M.; Thomann, Y.; Kubler, R.; Mulhaupt, R. *Adv. Funct. Mater.* **2008**, *18*, 2390.
(24) Sturcova, A.; Davies, G. R.; Eichhorn, S. J. *Biomacromolecules* **2005**, *6*, 1055.
(25) Rusli, R.; Eichhorn, S. J. *Appl. Phys. Lett.* **2008**, 93.
(26) Lu, J.; Askeland, P.; Drzal, L. T. *Polymer* **2008**, *49*, 1285.
(27) Steinmann, B. U.S. Patent 005972563A, 1999.
(28) Kharchenko, S. B.; Douglas, J. F.; Obrzut, J.; Grulke, E. A.; Migler, K. B. *Nat. Mater.* **2004**, *3*, 564.
(29) Hu, G. J.; Zhao, C. G.; Zhang, S. M.; Yang, M. S.; Wang, Z. G. *Polymer* **2006**, *47*, 480.
(30) Du, F. M.; Scogna, R. C.; Zhou, W.; Brand, S.; Fischer, J. E.; Winey, K. I. *Macromolecules* **2004**, *37*, 9048.
(31) Ben Mabrouk, A.; Magnin, A.; Belgacem, M. N.; Boufi, S. *Compos. Sci. Technol.* **2011**, *71*, 818.
(32) Siqueira, G.; Mathew, A. P.; Oksman, K. *Compos. Sci. Technol.* **2011**, *71*, 1886.
(33) Coleman, J. N.; Khan, U.; Blau, W. J.; Gun'ko, Y. K. *Carbon* **2006**, *44*, 1624.
(34) Eichhorn, S. J.; Dufresne, A.; Aranguren, M.; Marcovich, N. E.; Capadona, J. R.; Rowan, S. J.; Weder, C.; Thielemans, W.; Roman, M.; Renneckar, S.; Gindl, W.; Veigel, S.; Keckes, J.; Yano, H.; Abe, K.; Nogi, M.; Nakagaito, A. N.; Mangalam, A.; Simonsen, J.; Benight, A. S.; Bismarck, A.; Berglund, L. A.; Peijs, T. *J. Mater. Sci.* **2010**, *45*, 1.
(35) Yeh, M. K.; Tai, N. H.; Liu, J. H. *Carbon* **2006**, *44*, 1.
(36) Montazeri, A.; Montazeri, N. *Mater. Des.* **2011**, *32*, 2301.
(37) Visakh, P. M.; Thomas, S.; Oksman, K.; Mathew, A. P. *Compos., Part A* **2012**, *43*, 735.
(38) Gong, G.; Pyo, J.; Mathew, A. P.; Oksman, K. *Compos., Part A* **2011**, *42*, 1275.
(39) Jonoobi, M.; Harun, J.; Mathew, A. P.; Oksman, K. *Compos. Sci. Technol.* **2010**, *70*, 1742.
(40) Mendez, J.; Annamalai, P. K.; Eichhorn, S. J.; Rusli, R.; Rowan, S. J.; Foster, E. J.; Weder, C. *Macromolecules* **2011**, *44*, 6827.